

High Time Resolution Observations of Magnetospheric Disturbances During Auroral Activity

M. O. Fillingim,¹ G. K. Parks,¹ R. P. Lin,¹ M. McCarthy,² and A. Szabo³

Abstract.

We present high time resolution plasma and magnetic field data from the near-Earth plasma sheet during times of active aurorae. The plasma sheet disturbance associated with the auroral activity is composed of Earthward traveling ions with large mean velocities ($\langle \mathbf{v} \rangle = \int \mathbf{v} f(\mathbf{v}) d^3v$) and large amplitude, high frequency magnetic field fluctuations. The ion $\langle \mathbf{v} \rangle$ can change substantially (by up to 100%) on time scales comparable to the local proton gyroperiod. The magnetic fluctuations lead to large, rapidly varying induced electric fields. Power spectral analysis of the magnetic field data shows a significant amount of wave power present at frequencies up to and greater than the local proton cyclotron frequency. Examination of the three-dimensional ion distribution functions indicates that the distributions are complex and nongyrotropic, with large gradients and anisotropies, and dynamic, with considerable changes in the phase space features within one gyroperiod. These results illustrate that kinetic physics controls the plasma behavior during times of plasma sheet disturbances associated with auroral activity. This conclusion is in contrast to the usual interpretation that the large ion velocity moments observed during plasma sheet disturbances are convective in nature (i.e., bursty bulk flows). Additionally, we show that these kinetic effects are important in the near-Earth plasma sheet over a wide range of geomagnetic activity, from pseudobreakups to substorms. Therefore, we suggest that these kinetic processes operate during all types of geomagnetic disturbances and can occur throughout large regions of the magnetotail during substorms and storms.

1. Introduction

Aurorae come in a large variety of spatial sizes and intensities, from the smallest pseudobreakup to large scale substorms to storm-time aurora which may extend down to mid-latitudes. Three examples of different levels of auroral activity are shown in Figure 1. The image on the far left illustrates a pseudobreakup. The region of intense auroral emission is limited to only a few degrees in latitude and a few hours of local time. Additionally, the duration of the emission is very short, on the order of a few minutes. In this case the strength of the geomagnetic disturbance was quite weak. The AE index was < 100 nT and the K_P index was 1^- .

The middle image shows a moderate substorm near the end of the expansive phase when the area of the active aurora reaches its maximum size. The region of intense emission covers nearly the entire midnight sector, spanning 20° in latitude and over 6 hours of local time. The expansive phase of such a substorm can last an hour or more. For this particular substorm, the AE index reached ~ 400 nT and K_P was 3^- .

On the far right, the image shows the extent of energetic electron precipitation during a magnetospheric storm. The auroral emission

extends equatorward of 60° at all local times except near local noon and reaches poleward of 80° near midnight. Intense aurora associated with storms can last several hours to a significant fraction of a day. Storms produce strong geomagnetic disturbances. During the early phase of the storm when this image was taken, AE was ~ 2000 nT and K_P was high at 8^- . Several hours later D_{st} reached its minimum value of about -200 nT.

All of these auroral events are linked magnetically to the magnetosphere. Because of this, auroral images can be used to get a global view of magnetospheric disturbances. It is also invaluable to use *in situ* plasma and magnetic field data in the magnetosphere to get a local, detailed view of the processes involved. Several of our previous studies have combined global auroral images from POLAR/UVI [Torr *et al.*, 1995] and *in situ* plasma and magnetic field measurements from perigee passes of the WIND spacecraft through the near-Earth plasma sheet to form a coherent picture of how magnetospheric disturbances are related to auroral activity [Fillingim *et al.*, 2000, 2001; Parks *et al.*, 2001, 2002].

Both Fillingim *et al.* [2001] and Parks *et al.* [2002] have recently shown that the plasma dynamics in the plasma sheet appear the same during pseudobreakups and substorms. The left hand side of Figure 2 shows four hours of auroral and plasma sheet data during a series of pseudobreakups observed on 26 July 1997. The right hand side shows data from two large substorms observed over seven hours on 27 March 1997. (See Figure 1, left and middle images.) Both panels show, from top to bottom, a keogram (auroral intensity as a function of latitude and Universal Time) centered on local midnight constructed from UVI images with the latitudinal position of the WIND footprint marked; the energy deposition rate computed from UVI images in units of gigawatts carried by precipitating electrons into the nightside ionosphere; the plasma sheet magnetic field measured by WIND/MFI [Lepping *et al.*, 1995] in GSM coordinates; the ion velocity moment computed from the three-dimensional distributions measured by WIND/3DP [Lin *et al.*, 1995] in GSM coordinates; the ion velocity in magnetic field aligned coordinates;

¹Space Sciences Laboratory, University of California, Berkeley, California, USA.

²Department of Earth and Space Sciences, University of Washington, Seattle, Washington, USA.

³Laboratory for Extraterrestrial Physics, NASA Goddard Space Flight Center, Greenbelt, Maryland, USA.

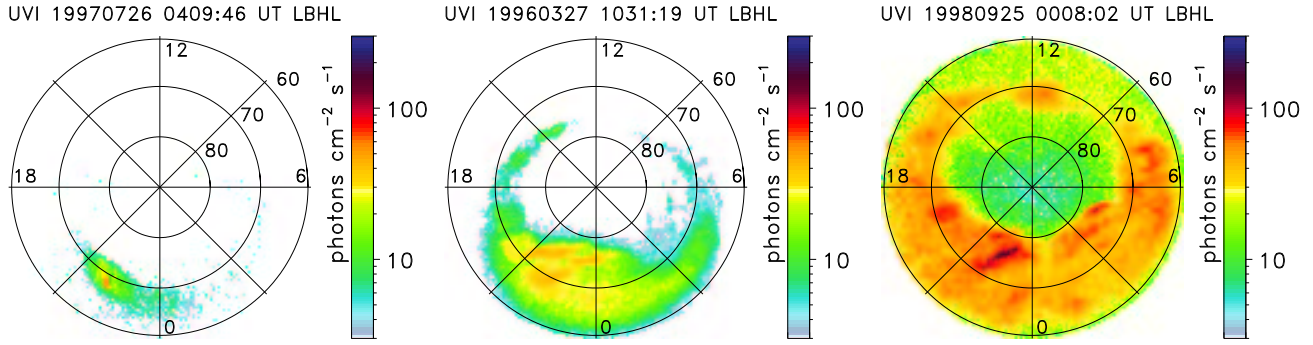


Figure 1. Examples of different levels of auroral activity. From left to right: pseudobreakup, substorm, storm.

and the omnidirectional ion flux in units of $(\text{cm}^2\text{-sec-ster-keV})^{-1}$ at four different energies from 10 keV to 1 MeV. During the four hour period on 26 July 1997, the footprint of WIND moved from a local time of 21 to midnight at a radius of 11 R_E . For the interval shown from 27 March 1996, the WIND footprint moved from a local time of 20:30 to 22:30 at a radius of about 17 R_E .

An important feature to note is that when the footprint of WIND maps to the region of intense auroral emission, several repeatable phenomena are seen. These include large ion velocity moments ($\langle \mathbf{v} \rangle = \int \mathbf{v} f(\mathbf{v}) d^3v$) typically in the Earthward direction at WIND perigee distances of -10 to $-20 R_E$ with, at times, a sizable com-

ponent directed parallel to the magnetic field; large amplitude, high frequency fluctuations in all three components of the magnetic field; and increases in the energetic ion (electron) fluxes up to MeV (several hundred keV) energies. These phenomena appear quite similar in the plasma sheet even though the auroral activity is quite different.

Many of the same features in the plasma sheet have been noted by *Angelopoulos et al.* [1997] and *Fairfield et al.* [1999] in conjunction with substorm onsets and intensifications identified using global auroral images. The typical interpretation for the large ion velocity moments is that they are caused by an enhanced, quasi-static electric field resulting in a large $\mathbf{E} \times \mathbf{B}$ drift. That is, they are due to enhanced convection and have been termed burst bulk flows (BBFs) [Angelopoulos et al., 1992]. The electric field that would

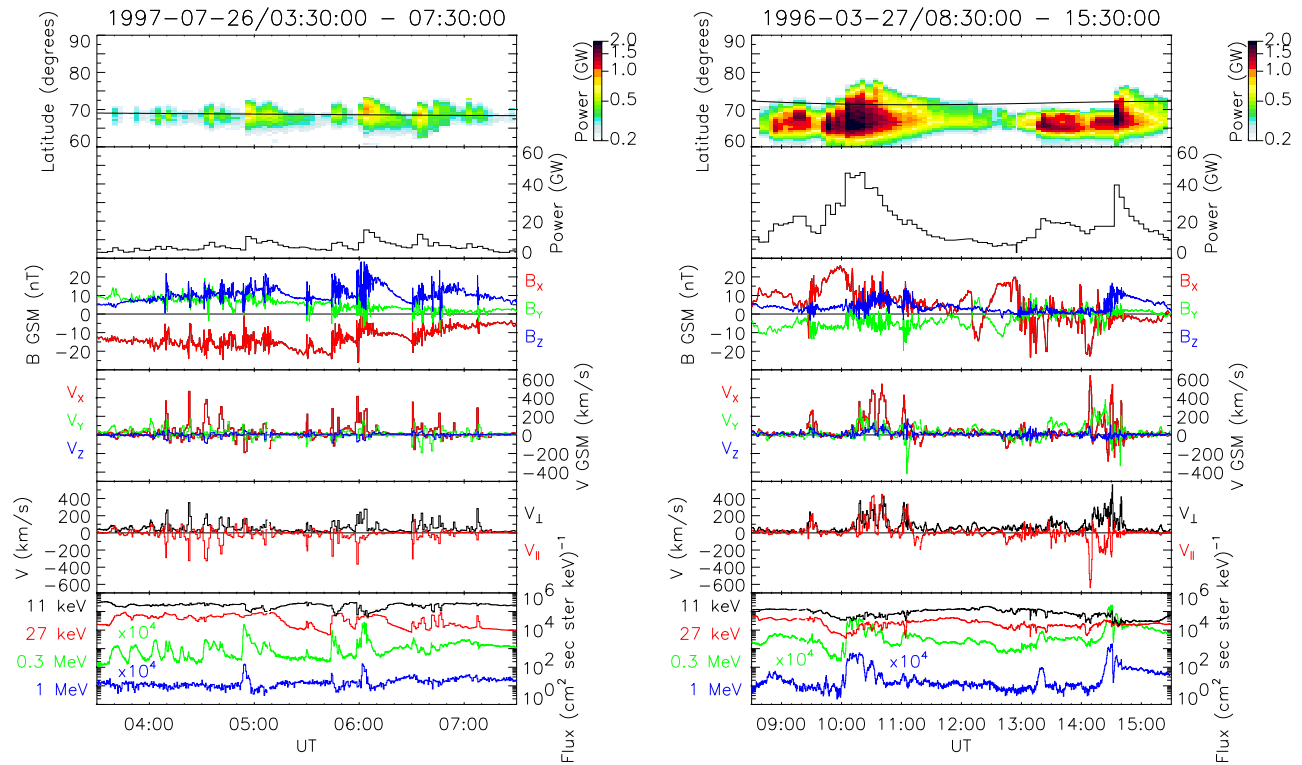


Figure 2. Auroral and plasma sheet data from a series of pseudobreakups (left) and a sequence of substorms (right). From top to bottom: keogram, energy deposition rate in the the nightside ionosphere (both computed from UVI images), GSM components of the plasma sheet magnetic field, GSM components of the ion velocity moment, ion (\mathbf{v}) in magnetic field aligned coordinates, and omnidirectional ion flux (bottom four panels measured by WIND).

be necessary to produce the observed $\langle \mathbf{v} \rangle$ is about 5 to 10 mV/m ($\mathbf{E} = -\langle \mathbf{v} \rangle \times \mathbf{B}$), roughly an order of magnitude larger than typical estimates for the cross tail convection electric field. BBFs have been interpreted to be the result of reconnection in the tail and have been invoked to explain the bulk transport of mass, energy, and flux from the tail to the near-Earth region.

However, close examination of the particle distribution functions during both pseudobreakups and substorms shows that the distributions can be quite complex and indicates that the large $\langle \mathbf{v} \rangle$ are mainly due to highly anisotropic energetic ions. Figure 3 shows some representative ion distribution functions. Two-dimensional slices of the three-dimensional distribution functions in the $\mathbf{B} - \mathbf{V}_\perp$ plane in the spacecraft frame of reference are shown along with one-dimensional cuts in the directions parallel (red asterisks) and perpendicular (blue diamonds) to the averaged magnetic field. The horizontal axis in the contour plots is velocity parallel to \mathbf{B} while the vertical axis is velocity perpendicular. The numbers in the upper left, upper right, and lower right of the contour plots are the elevation angle, azimuth angle, and magnitude of the magnetic field averaged over the integration time (50 seconds, except for the lower right distribution which is integrated over 25 seconds). The plus signs in each contour plot indicates the direction and magnitude of $\langle \mathbf{v} \rangle$. The horizontal axis in the 1-D cuts is velocity; the vertical axis

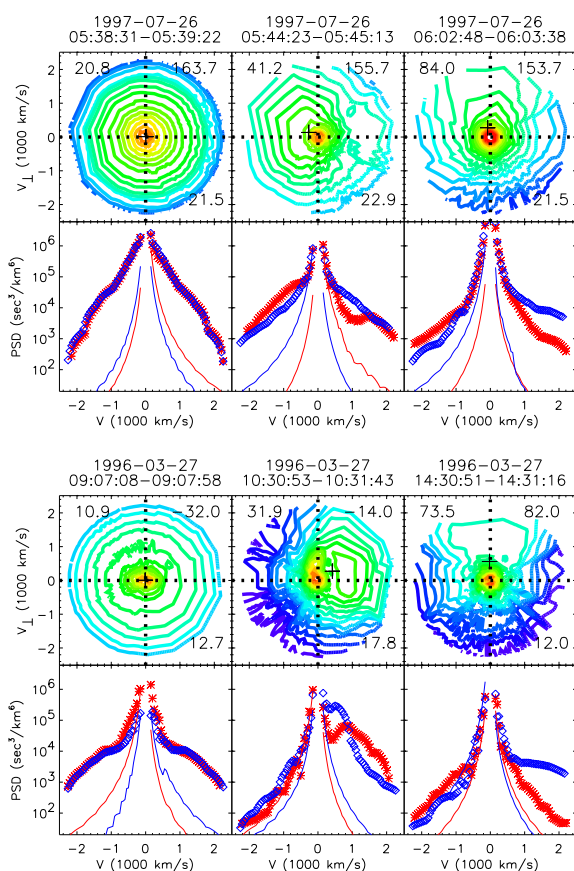


Figure 4. Ion phase space velocity distribution functions before and during large $\langle \mathbf{v} \rangle$ associated with pseudobreakups (top row) and substorms (bottom row). The contour plots show 2-D slices of the 3-D distribution in the $\mathbf{B} - \mathbf{V}_\perp$ plane in the spacecraft frame. The line plots show 1-D cuts parallel (red asterisks) and perpendicular (blue diamonds) to \mathbf{B} .

is the phase space density in units of s^3km^{-6} . The solid red and blue lines represent the one-count level in that particular direction. Since the detector has a variable angular resolution depending upon look direction, the one-count level depends upon look direction. The top three contour plots and 1-D cuts show data from pseudobreakups observed on 26 July 1997 while the bottom plots contain data obtained during substorms on 27 March 1996.

The first column shows the ion distributions when WIND does not map to the region of intense auroral emission. The distributions appear relatively isotropic, though there are clearly two populations present. The two component nature of the distributions is most visible in the bottom most plots where the break in the spectrum occurs at ~ 5 keV or about 1000 km/s (assuming the ions are protons).

The plots in the middle column again illustrate the multi-component nature of the ion distributions. Additionally, they show that the different components may behave dynamically differently. In both cases, there is a parallel beam present along with a core population. In the top example, a parallel beam with an energy of about 10 keV is present along with a relatively energetic ion population that is shifted anti-parallel and somewhat perpendicular to the magnetic field (upper left quadrant) as indicated by $\langle \mathbf{v} \rangle$. The beam does not appear shifted in the perpendicular direction. The bottom distribution in the middle column similarly contains a wide parallel beam with an energy of about 5 keV. A very low energy, anisotropic population is also present. The low energy population is shifted slightly in the anti-parallel direction. Both the core and the beam are shifted by a few hundred km/s in the perpendicular direction suggesting that the plasma is being convected by an electric field.

The distributions in the last column are highly anisotropic and appear nongyrotropic at energies greater than a few keV. The energetic populations are shifted perpendicular to \mathbf{B} relative to the spacecraft, and steep phase space density gradients are present. The 1-D cuts show plateaus extending to the highest energy channels of the detector (> 30 keV). *Chen et al.* [2000b] have shown that the anisotropy can persist up to MeV energies.

These examples show how the single component fluid assumption [*Nakamura et al.*, 1991] can breakdown in the plasma sheet during active intervals. The computed velocity moments in these cases do not accurately represent the plasma behavior. Multi-component distributions in which the different populations are behaving dynamically differently cannot be adequately explained solely by convection. Other processes must be operating to create these complex and dynamic distributions with multiple populations, beams, and strong phase space density gradients. It is for this reason that we do not refer to these events as BBFs. The $\langle \mathbf{v} \rangle$ are not due to the bulk motion of a single component plasma and are not flows in the sense that motion is only perpendicular to \mathbf{B} .

The similarity of the phase space features present in the distributions during pseudobreakups and substorms leads us to conclude that the same, as yet unidentified, physical processes are operating in the plasma sheet during both types of auroral activity. *Parks et al.* [2002] extended this line of reasoning and suggested that just as there is a continuum of scale sizes and intensities of auroral activity, there is a continuum of scale sizes and intensities of plasma sheet disturbances. During a pseudobreakup only a small region of the plasma sheet is affected. A much larger region of the plasma sheet is disturbed during substorms, but the same physical mechanisms are operating. If we extrapolate this idea to storms, then the same processes may be active throughout nearly the entire nightside plasma sheet.

These previous conclusions were reached using plasma data integrated over several to several tens of ion gyroperiods which give only an average picture of the ion dynamics. In the next section, we

show high resolution plasma data with a temporal resolution on the order of the proton gyroperiod. These data strongly demonstrate that the processes involved in plasma sheet disturbances associated with auroral activity are kinetic and nonlinear. Our observations stress the importance of using high time resolution measurements to get a clear picture of the dynamics that are active in the plasma sheet during pseudobreakups, substorms, and storms.

2. Observations

2.1. Pseudobreakup: 26 July 1997

On 26 July 1997, WIND was in the near-Earth plasma sheet at a radial distance of about 11 R_E while POLAR/UVI was imaging the entire northern auroral region. As shown in the left hand side of Figure 2, between 03:00 and 08:00 UT the WIND plasma and magnetic field instruments recorded a series of plasma sheet disturbances each composed of large Earthward ion $\langle \mathbf{v} \rangle$, large amplitude, high frequency magnetic field fluctuations, and increases in the flux of energetic particles. At the same time, POLAR/UVI observed a series of minor auroral brightenings interpreted as pseudobreakups coincident with the plasma sheet disturbances. *Fillingim et al. [2000]* gives an overview of these observations. Here we focus on high resolution data during one event near 06:30 UT.

Figure 4 shows a detailed look at the ion $\langle \mathbf{v} \rangle$ and magnetic field variations during the seven minute period from 06:29 to 06:36 UT. At this time, WIND was at a GSM position of $[-11, 2, 0.5] R_E$ which translates to a magnetic local time of 23:30. The figure shows, from top to bottom, the components of $\langle \mathbf{v} \rangle$ in GSM coordinates (plus $|\langle \mathbf{v} \rangle|$), $\langle \mathbf{v} \rangle$ in magnetic field aligned coordinates, three components of the magnetic field in GSM coordinates, the time derivative of the magnitude of the magnetic field, and a dynamic frequency spectrogram of the magnetic field.

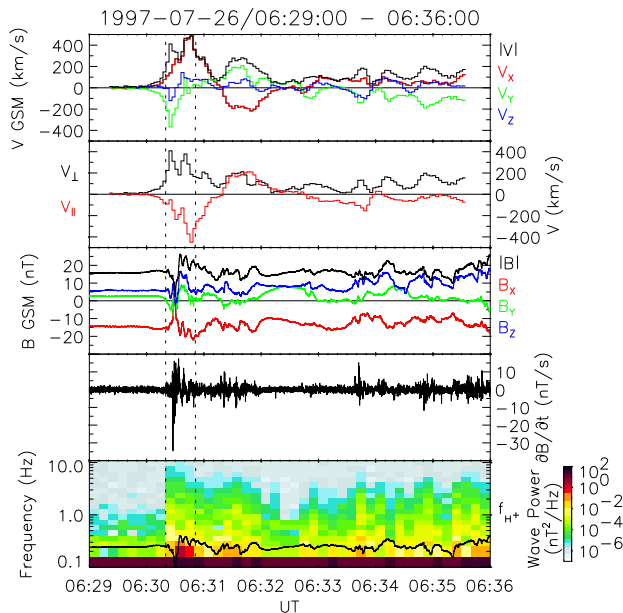


Figure 3. Plasma sheet ion and magnetic field data. From top to bottom: ion $\langle \mathbf{v} \rangle$ in GSM coordinates (plus $|\langle \mathbf{v} \rangle|$), ion $\langle \mathbf{v} \rangle$ in magnetic coordinates, GSM components of \mathbf{B} (plus $|\mathbf{B}|$), $\partial|\mathbf{B}|/\partial t$, dynamic frequency spectrogram.

The $\langle \mathbf{v} \rangle$ are calculated from the three-dimensional ion distribution functions integrated over 3.1 seconds (one spacecraft rotation) which were continuously sampled for the entire nearly seven minute interval. This integration time is comparable to the local proton gyroperiod. The magnetic field data has a time resolution of 0.046 seconds. The dynamic frequency spectrogram was created by computing the Fast Fourier Transform for every 10 second segment of magnetic field data. The wave power in nT^2/Hz is plotted as a function of frequency from about 11 Hz (the Nyquist frequency) to 0.1 Hz and UT. The solid black line represents the local proton gyrofrequency. Note that there is a 3 second sinusoidal variation in \mathbf{B} before 06:30 UT due to the spacecraft rotation. As a result, there is a horizontal band centered on 0.3 Hz and a weaker band centered on 0.6 Hz before 06:30 UT in the dynamic frequency spectrogram.

An important feature in this figure is the large changes seen in $\langle \mathbf{v} \rangle$ on time scales comparable to the proton gyroperiod. Before 06:30:10 $\langle \mathbf{v} \rangle$ increases very gradually, primarily in the $-Y$ -direction. At 06:30:25, the component of the velocity perpendicular to \mathbf{B} (mostly in the $-Y$ -direction) increases by almost 100% in 3.1 seconds. The X -component of $\langle \mathbf{v} \rangle$ increases by 50% near 06:30:40. Two peaks are also present in $|\langle \mathbf{v} \rangle|$ within a few gyroperiods of each other. The first peak is centered about 06:30:25 UT and is directed mainly in the $-Y$ -direction with a smaller $-Z$ -component. This leads to a velocity perpendicular to the ambient magnetic field. The second peak is centered around 06:30:45 UT and is directed largely in the X -direction. During this second peak, as the direction of \mathbf{B} changes, the velocity is first directed perpendicular then parallel to the magnetic field. In this case, the direction of $\langle \mathbf{v} \rangle$ does not appear to be constrained by the direction of \mathbf{B} .

The rapid, large amplitude variations in the magnetic field on time scales faster than the proton gyroperiod can be clearly seen throughout this interval. Starting around 06:30:20 UT, small oscillations with periods less than one second are seen in all three components of the magnetic field. As the magnitude of \mathbf{B} decreases, the oscillations continue, and, in the Z -component, the amplitude of the oscillations grow. Near 06:30:30 UT $|\mathbf{B}|$ reaches its minimum as B_x briefly changes sign indicating that WIND may have crossed a current sheet or encountered strong local turbulence. There is also a brief excursion of B_z to negative values just after the B_x sign change during the period of Earthward dominated $\langle \mathbf{v} \rangle$. As $|\mathbf{B}|$ increases, mainly due to increases in B_x and B_z , short period magnetic oscillations are present. The amplitude of the change in $|\mathbf{B}|$ is greater than 20 nT, larger than the original magnetic field strength. Since $\Delta B/B$ is greater than unity, this suggests that the instability is nonlinear.

$\partial B/\partial t$ can get quite large with a peak near -35 nT/s . More typical values are on the order of 10 nT/s. This translates to induced electric field strengths of several to 10 mV/m at scale lengths of the thermal proton gyroradius (several hundred km).

The dynamic frequency spectrogram shows significant wave power up to and exceeding the local proton gyrofrequency. The sharp decrease in $|\mathbf{B}|$ at 06:30:30 UT results in a broadband frequency response; however, short period oscillations are seen before, during, and after this spike. Wave power exists at frequencies up to and exceeding the proton gyrofrequency for several minutes. Since the fastest proton gyroperiod during this interval is about 2.5 seconds, and the more typical value is 4 seconds, the ions cannot be behaving adiabatically during such large magnetic field changes over such short time scales.

Phase space velocity distribution functions during the interval of large $\langle \mathbf{v} \rangle$ are presented in Figure 5. Ten two-dimensional slices of the 3-D distribution functions in the $\mathbf{B} - \mathbf{V}_\perp$ plane in the spacecraft frame of reference are again shown along with 1-D cuts. The format is the same as that in Figure 3, except that the distributions are

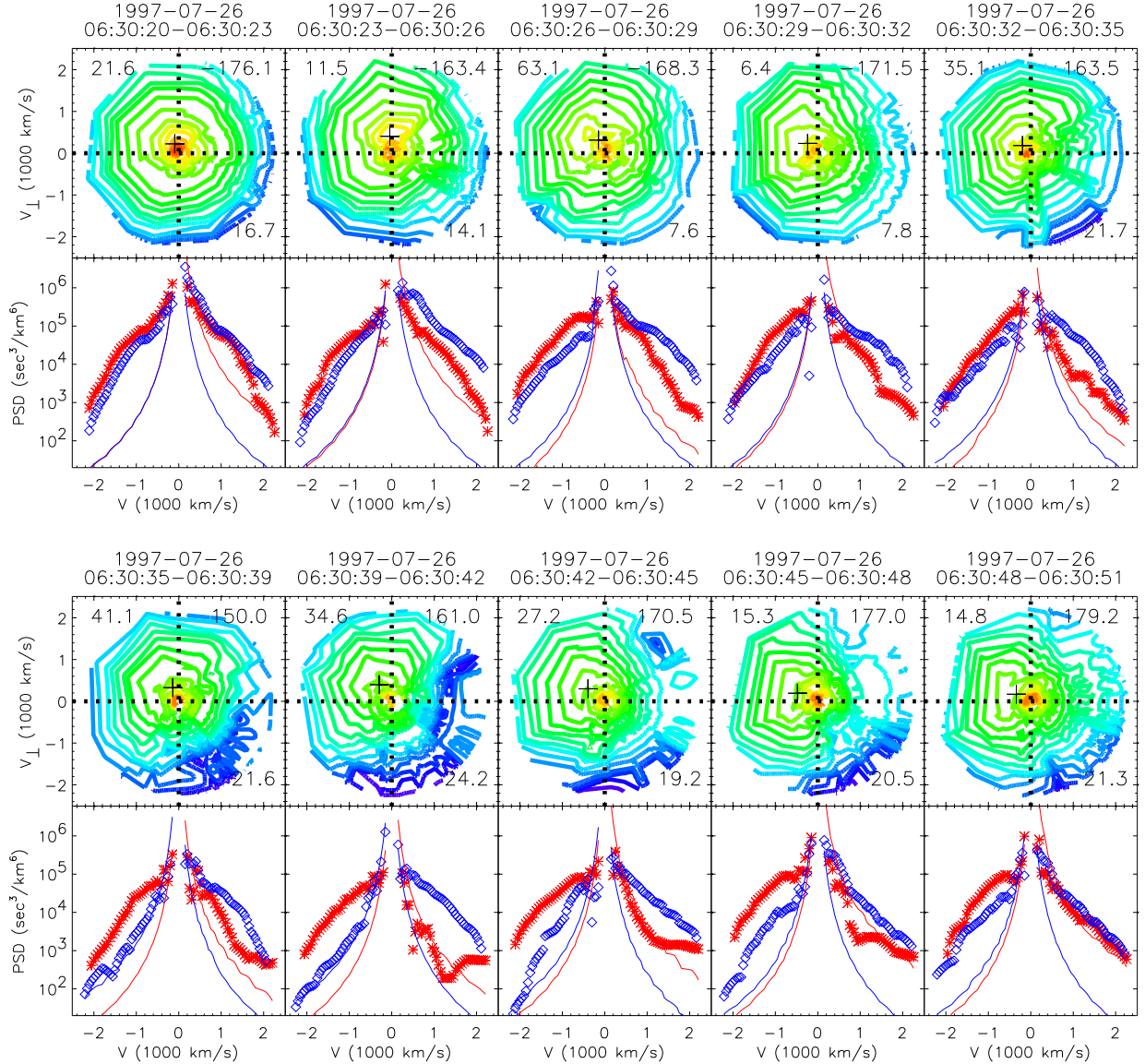


Figure 5. Ion phase space velocity distribution functions during the interval of large $\langle \mathbf{v} \rangle$.

integrated over 3.1 seconds. The vertical dashed lines in Figure 4 show the interval in which these distributions are taken. The second contour plot corresponds to the first peak in $|\langle \mathbf{v} \rangle|$ and v_{\perp} and the negative peak in $\langle \mathbf{v} \rangle_{\mathbf{v}}$ in Figure 4.

The first distribution in this figure appears nearly isotropic in the plasma frame. There is a shift in the distribution toward the upper left quadrant resulting in a $\langle \mathbf{v} \rangle$ of just over 200 km/s, but the contours are nearly circular and concentric. It appears as though two components are present. There is a “ledge” in the distribution near 1000 km/s. It is also apparent in the 1-D cuts as a break in the spectrum. This feature is seen in earlier distributions as well.

From the first to the second distribution, the $|\langle \mathbf{v} \rangle|$ nearly doubles to over 400 km/s. The second distribution is much more complex and anisotropic; sharp gradients in the phase space density are present. There is an enhancement of high energy particles perpendicular to the magnetic field which gives rise to the first peak in $\langle \mathbf{v} \rangle$. A Galilean transformation of an isotropic distribution can-

not reproduce the features seen here. However, the magnetic field is changing during the 3.1 second integration time, so some time aliasing may be occurring.

Notice that from the fifth to the sixth distribution, there is a large decrease in the phase space density of high energy particles in the lower right quadrant, which corresponds to particles traveling in the tailward direction. The phase space density decreases by an order of magnitude at 10 keV in this direction in one gyroperiod. A careful analysis shows that the decrease in this direction is not as extreme at higher and lower energies.

In the last five distributions, note how the direction of the enhancement in energetic particles and $\langle \mathbf{v} \rangle$ as indicated by the plus sign changes from mostly perpendicular to \mathbf{B} to nearly parallel to \mathbf{B} . At the same time, the elevation angle of \mathbf{B} changes from about 40° to 14° while the azimuthal angle remains fairly constant. However, note that, as shown in the top panel of Figure 4, $\langle \mathbf{v} \rangle$ is directed almost entirely in the X -direction throughout this time interval.

(The seventh, eighth, and ninth distributions represent the second, broad peak in $\langle \mathbf{v} \rangle$ and the peak in the X -component of $\langle \mathbf{v} \rangle$.) Therefore, the direction of $\langle \mathbf{v} \rangle$ is not changing while the direction of \mathbf{B} is changing. It appears that the ion dynamics at this point are not controlled by the local magnetic field.

2.2. Substorm: 30 September 1997

For completeness we also present high resolution data obtained during a substorm observed on 30 September 1997. At 04 UT on 30 September 1997, WIND was located at a GSM position of $[-14, 5, -2] R_E$, a magnetic local time of about 22:30. When UVI begins observing the aurora shortly before 04 UT, a substorm is already in progress. Ground magnetograms suggest that the substorm onset (and a subsequent intensification) may have occurred between 03 and 04 UT. Figure 6 shows high resolution plasma sheet ion and magnetic field data from a time when WIND mapped to the region of active aurora during this substorm. The format of Figure 6 is identical to that of Figure 4. Again the ion data have a resolution of 3.1 seconds (one spacecraft rotation) and the magnetic field data have a resolution of 0.046 seconds.

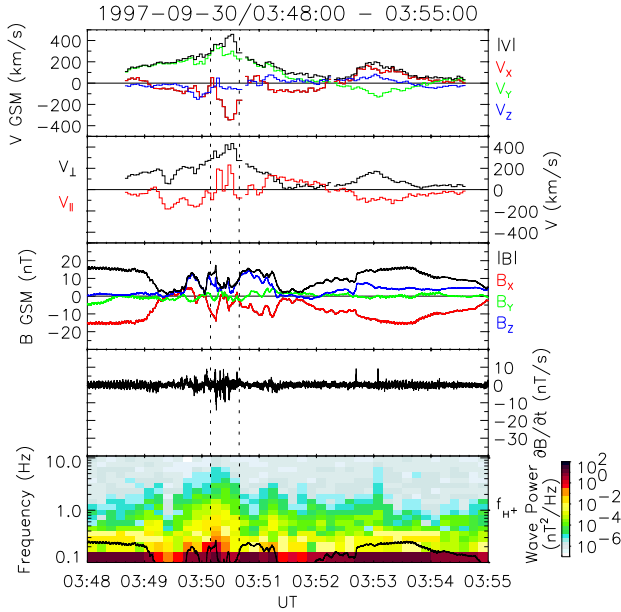


Figure 6. Same as Figure 4.

There is some interesting behavior seen in the ion velocity moments. At the beginning of this interval, the ion $\langle \mathbf{v} \rangle$ is already elevated (> 100 km/s), pointed mostly in the Y -direction, and gradually increasing. The $\langle \mathbf{v} \rangle$ is directed mostly perpendicular to \mathbf{B} . As the velocity peaks in the Y -direction, the $-X$ -component of $\langle \mathbf{v} \rangle$ rapidly increases and peaks at over 300 km/s in about 10 seconds. $|\mathbf{v}|$ and v_{\perp} also peak at this time. Subsequently, the $-\langle \mathbf{v} \rangle_x$ component quickly decreases. Since \mathbf{B} is between 5 and 10 nT, the duration of the $-\langle \mathbf{v} \rangle_x$ increase and decrease is just a few gyroperiods.

The bottom three panels show that the magnetic field is highly variable during this interval. B_x changes sign several times between 03:49 and 03:52 UT, indicating either multiple crossings of the current sheet or strong local turbulence. The minimum value of $|\mathbf{B}|$ is about 1 nT, indicating that WIND is near the neutral sheet. $\partial B/\partial t$ routinely reaches values on the order of 10 nT/s. While

smaller than the peak values observed on July 26, 1997, the induced electric field can still be ~ 10 mV/m at length scales of the gyroradii of the thermal protons. Similar to July 26, 1997, the dynamic frequency spectrogram shows that there is wave power at and above the local proton gyrofrequency throughout this interval.

Ten three-second resolution ion distribution functions are shown in Figure 7. These distributions cover the time interval of the $-X$ -component of $\langle \mathbf{v} \rangle$. Again the dashed vertical lines in Figure 6 show the interval from which these distributions are taken.

The first two distributions are quite energetic with very few particles with energies below about 1 keV (~ 500 km/s) present. The distributions are anisotropic in the direction perpendicular to the magnetic field. In the third distribution, the phase space density of ions with energies around a few keV increases noticeably. This increase is most clearly seen in the upper right quadrant. This lower energy but anisotropic component which is responsible for the $-\langle \mathbf{v} \rangle_x$ persists for the next six distributions. Throughout these seven distributions, the direction of the $\langle \mathbf{v} \rangle$ does not change; it remains pointed duskward and tailward. However, the direction of $\langle \mathbf{v} \rangle$ as indicated by the small crosses in the contour plots does change as the magnetic field changes direction. In the final distribution, the medium energy component disappears leaving the anisotropic energetic component and a $\langle \mathbf{v} \rangle_y > 200$ km/s behind.

3. Discussion

The processes occurring during high ion $\langle \mathbf{v} \rangle$ events in the near-Earth plasma sheet are dynamic and possibly nonlinear. Here and in our previous work we have shown that large $\langle \mathbf{v} \rangle$ events are associated with anisotropic, complex ion distribution functions, increases in the flux of energetic particles up to MeV energies, large amplitude, high frequency magnetic field fluctuations, and intense aurora in the ionosphere [Chen *et al.*, 2000a, b; Fillingim *et al.*, 2000, 2001; Parks *et al.*, 2001, 2002]. Here we have shown high time resolution ion and magnetic field data from large ion $\langle \mathbf{v} \rangle$ events in the near-Earth plasma sheet associated with auroral activity to demonstrate that additional features are present. For example, large ion $\langle \mathbf{v} \rangle$ can contain significant structure, that is, multiple peaks in $|\langle \mathbf{v} \rangle|$ separated in time by a few proton gyroperiods and abrupt changes (up to 100%) in both the direction and magnitude of $\langle \mathbf{v} \rangle$ on time scales comparable to the local proton gyroperiod.

At the same time, large amplitude, high frequency magnetic field fluctuations are seen with $|\partial B/\partial t|$ typically reaching ~ 10 nT/s. These magnetic field fluctuations will give rise to strong, rapidly changing induced electric fields. At scale lengths on the order of the gyroradius of a 1 keV proton (several hundred km in a 10 to 20 nT field), the induced electric field strength will be on the order of 10 mV/m. This is at least an order of magnitude larger than typical expected dawn-to-dusk electric fields of a few tenths of mV/m and is similar in magnitude to $\langle \mathbf{v} \rangle \times \mathbf{B}$ (500 km/s $\times 20$ nT = 10 mV/m), which is usually interpreted as an enhanced convective electric field. However, the induced electric fields, rather than being quasi-static in the Y -direction for Earthward transport, are rapidly changing in direction and magnitude as \mathbf{B} varies on time scales faster than the proton gyroperiod.

These magnetic fluctuations have significant wave power present at frequencies up to and exceeding the local proton gyrofrequency. Lui *et al.* [1992] saw similar broadband increases in wave power at similar locations and interpreted their observations as a signature of a cross field current instability giving rise to current disruption. Perraut *et al.* [2000] have also noted enhanced wave power at and above the proton gyrofrequency at geosynchronous altitudes which may be related to a parallel current-driven instability.

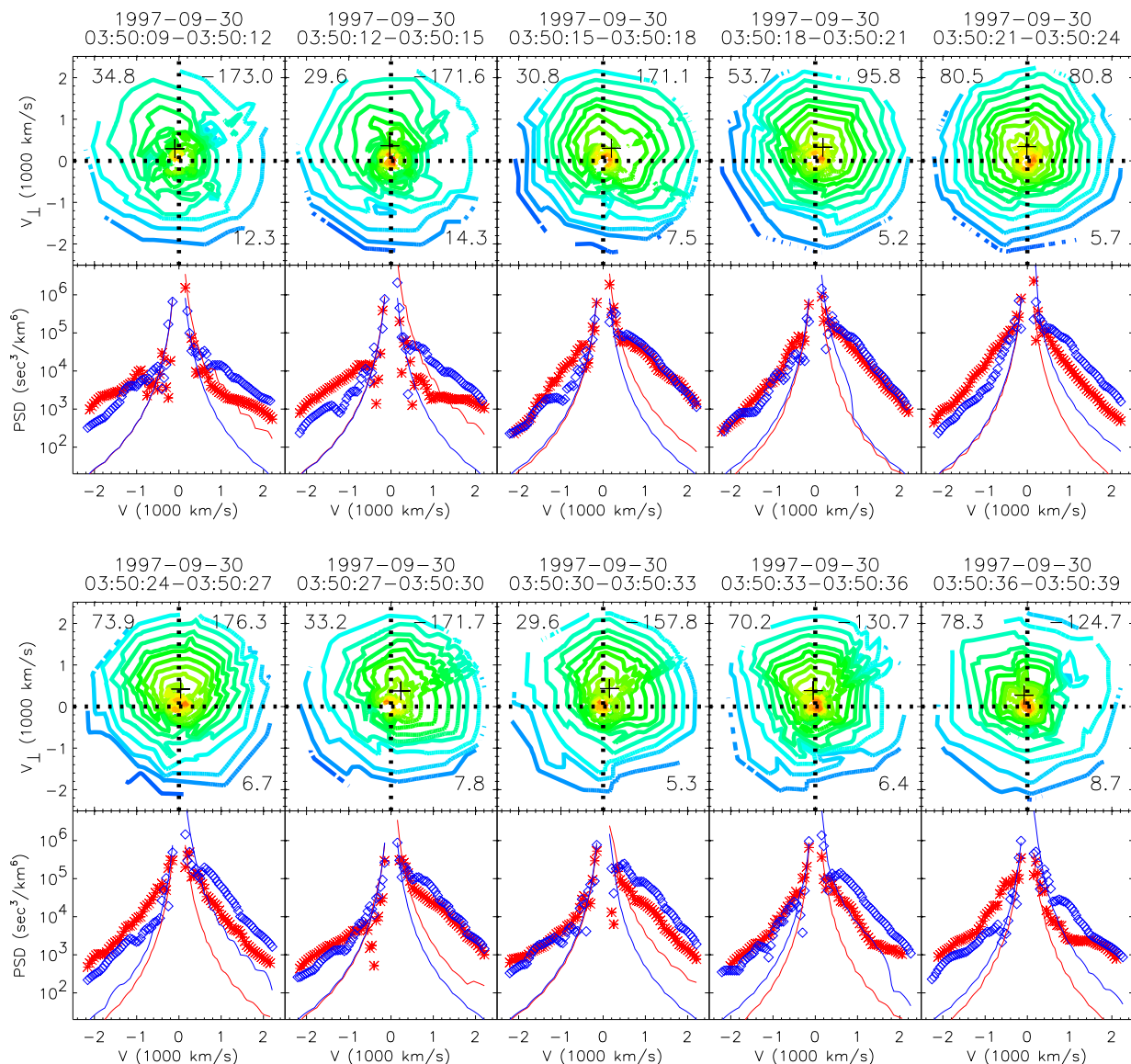


Figure 7. Same as Figure 5.

The ion distribution functions contain complex features that include large gradients and anisotropies in phase space. These features cannot be reproduced by a transformation of an isotropic distribution. Additionally, some of the features present appear nongyrotropic. Significant changes also occur in these distribution functions on time scales comparable to the local proton gyroperiod indicating that the plasma is very dynamic. It is clear from the rapid fluctuations in \mathbf{B} and from the changes in the ion distribution functions that the ions cannot be behaving adiabatically. Furthermore, the direction of $\langle \mathbf{v} \rangle$ at times is not affected by changes in the direction of \mathbf{B} , suggesting that the ions also may not be magnetized.

All of these observations taken together strongly indicate that kinetic processes are operating during periods of large $\langle \mathbf{v} \rangle$. *Chen et al.* [2000a, b] and *Parks et al.* [2001] have also argued that kinetic effects are important during large ion $\langle \mathbf{v} \rangle$ in the near-Earth plasma sheet. They found that the ion distributions contained multiple species, including those from the ionosphere. The measured $\langle \mathbf{v} \rangle$

were not always in agreement with the $\mathbf{E} \times \mathbf{B}$ convection velocity determined by analyzing the distributions. The exact kinetic processes operating have not yet been identified, but this is an area of continuing work.

The evidence presented here suggests that the large ion velocities may not be convective in nature as usually assumed. The interpretation that large ion $\langle \mathbf{v} \rangle$ are BBFs is based on lower resolution moment data [*Angelopoulos et al.*, 1992], not on gyroperiod resolution distribution functions. If large $\langle \mathbf{v} \rangle$ are not due to enhanced convection, then the role of BBFs as a transport mechanism of mass, energy, and flux from the tail to the near-Earth region will have to be reexamined.

With measurements from a single spacecraft, it is impossible to distinguish between spatial and temporal variations. However, the dynamic nature of the distributions, the large $\partial B/\partial t$, and the close association with time varying phenomena such as the aurora as shown by *Fillingim et al.* [2000], lead us to interpret these observations as temporal variations in the properties of the local plasma.

Multipoint measurements by multiple spacecraft missions such as Cluster may help resolve this ambiguity.

Our previous work suggests that the microphysical processes occurring in the near-Earth plasma sheet on minute time scales during pseudobreakups and substorms appear to be the same [Fillingim *et al.*, 2001; Parks *et al.*, 2002]. We suggest that the processes occurring in the near-Earth plasma sheet on gyroperiod and subgyroperiod time scales are also a characteristic of all types of auroral activity. Analogous to the aurora, which is observed with a continuum of spatial and temporal scales, plasma sheet disturbances occur with a similar continuum of scales [Parks *et al.*, 2002]. The longer scales are used to describe the average behavior of the dynamics by means of MHD physics. But in smaller regions, MHD physics is not valid as the faster and small scale features become important. In these regions the physics must be characterized by kinetic processes. The kinetic processes, while still not fully understood, are important since they could be regulating and controlling many of the large-scale current and transport generation mechanisms. We have demonstrated that these kinetic processes occur in the near-Earth plasma sheet during pseudobreakups and substorms. We also propose that the same processes operate throughout much of the magnetotail during storms.

Acknowledgments. The Wind magnetometer data is courtesy of Ronald P. Lepping. This work was supported in part by NASA grants NAG5-3170 and NAG5-26580.

References

- Angelopoulos, V., W. Baumjohann, C. F. Kennel, F. V. Coroniti, M. G. Kivelson, R. Pellat, R. J. Walker, H. Lüher, and G. Paschmann, Bursty bulk flows in the inner central plasma sheet, *J. Geophys. Res.*, *97*, 4027, 1992.
- Angelopoulos, V., T. D. Phan, D. E. Larson, F. S. Mozer, R. P. Lin, K. Tsuruda, H. Hayakawa, T. Mukai, S. Kokubun, T. Yamamoto, D. J. Williams, R. W. McEntire, R. P. Lepping, G. K. Parks, M. Brittnacher, G. Germany, J. Spann, H. J. Singer, and K. Yumoto, Magnetotail flow bursts: association to global magnetospheric circulation, relationship to ionospheric activity and direct evidence for localization, *Geophys. Res. Lett.*, *24*, 2271, 1997.
- Chen, L., D. Larson, R. P. Lin, M. McCarthy, and G. Parks, Multicomponent plasma distributions in the tail current sheet associated with substorms, *Geophys. Res. Lett.*, *27*, 843, 2000a.
- Chen, L.-J., G. K. Parks, M. McCarthy, D. Larson, and R. P. Lin, Kinetic properties of bursty bulk flow events, *Geophys. Res. Lett.*, *27*, 1847, 2000b.
- Fairfield, D. H., T. Mukai, M. Brittnacher, G. D. Reeves, S. Kokubun, G. K. Parks, T. Nagai, H. Matsumoto, K. Hashimoto, D. A. Gurnett, and T. Yamamoto, Earthward flow bursts in the inner magnetotail and their relation to auroral brightenings, AKR intensifications, geosynchronous particle injections and magnetic activity, *J. Geophys. Res.*, *104*, 355, 1999.
- Fillingim, M. O., G. K. Parks, L. J. Chen, M. Brittnacher, G. A. Germany, J. F. Spann, D. Larson, and R. P. Lin, Coincident POLAR/UVI and WIND observations of pseudobreakups, *Geophys. Res. Lett.*, *27*, 1379, 2000.
- Fillingim, M. O., G. K. Parks, L. J. Chen, M. McCarthy, J. F. Spann, and R. P. Lin, Comparison of plasma sheet dynamics during pseudobreakups and expansive aurora, *Phys. Plasmas*, *8*, 1127, 2001.
- Lepping, R. P., M. H. Acuña, L. F. Burlaga, W. M. Farrell, J. A. Slavin, K. H. Schatten, F. Mariani, N. F. Ness, F. M. Neubauer, Y. C. Whang, J. B. Byrnes, R. S. Kennon, P. V. Panetta, J. Scheifele, and E. M. Worley, The WIND magnetic field investigation, *Space Sci. Rev.*, *71*, 207, 1995.
- Lin, R. P., K. A. Anderson, S. Ashford, C. Carlson, D. Curtis, R. Ergun, D. Larson, J. McFadden, M. McCarthy, G. K. Parks, H. Rème, J. M. Bosqued, J. Coutelier, F. Cotin, C. D'uston, K.-P. Wenzel, T. R. Sanderson, J. Henrion, J. C. Ronnet, and G. Paschmann, A three-dimensional plasma and energetic particle investigation for the WIND spacecraft, *Space Sci. Rev.*, *71*, 125, 1995.
- Lui, A. T. Y. R. E. Lopez, B. J. Anderson, K. Takahashi, L. J. Zanetti, R. W. McEntire, T. A. Potemra, D. M. Klumpar, E. M. Greene, and R. Strangeway, Current disruptions in the near-earth neutral sheet region, *J. Geophys. Res.*, *97*, 1461, 1992.
- Nakamura, M., G. Paschmann, W. Baumjohann, and N. Sckopke Ion distributions and flows near the neutral sheet, *J. Geophys. Res.*, *96*, 5631, 1991.
- Parks, G. K., L. J. Chen, M. Fillingim, and M. McCarthy, Kinetic characterization of plasma sheet dynamics, *Space Sci. Rev.*, *95*, 237, 2001.
- Parks, G. K., L. J. Chen, M. Fillingim, R. P. Lin, D. Larson, and M. McCarthy, A new framework for studying the relationship of aurora and plasma sheet dynamics, *J. Atmos. Terr. Phys.*, *64*, 115, 2002.
- Perraut, S., O. Le Contel, A. Roux, and A. Pedersen, Current-driven electromagnetic ion cyclotron instability at substorm onset, *J. Geophys. Res.*, *105*, 21,097, 2000.
- Torr, M. R., D. G. Torr, M. Zukic, R. B. Johnson, J. Ajello, P. Banks, K. Clark, K. Cole, C. Keffer, G. Parks, B. Tsurutani, and J. Spann, A far ultraviolet imager for the international solar-terrestrial physics mission, *Space Sci. Rev.*, *71*, 329, 1995.

M. McCarthy, Department of Earth and Space Sciences, University of Washington, Seattle, Washington 98195, USA.

M. O. Fillingim, R. P. Lin, G. K. Parks, Space Sciences Laboratory, University of California, Berkeley, California 94720, USA.

A. Szabo, Laboratory for Extraterrestrial Physics, NASA Goddard Space Flight Center, Greenbelt, Maryland, USA.

(Received _____.)